RESEARCH ARTICLE
ATMOSPHERIC PHYSICS

Earth and Planetary Physics
9: 1061–1072, 2025
doi: 10.26464/epp2025081

Remote influence of the Atlantic multidecadal oscillation on the autumn surface air temperature in Southwest China

WeiLing Xu[1], Yang Li[1*], QuanLiang Chen[1*], Xin Zhou[1], XingWen Jiang[2], Wei Wang[1], LiDou Huyan[3], Xiao Li[1], YangJie Jiang[1], RuiHan Deng[1], GuiPing Zhang[1], and Yun Zhu[4]

[1]Climate Change and Resource Utilization in Complex Terrain Regions Key Laboratory of Sichuan Province, School of Atmospheric Sciences, Chengdu University of Information Technology, Chengdu 610225, China;

[2]Heavy Rain and Drought-Flood Disasters in Plateau and Basin Key Laboratory of Sichuan Province, Institute of Tibetan Plateau Meteorology, China Meteorological Administration, Chengdu 610000, China;

[3]Chongqing Institute of Meteorological Sciences, Chongqing 404100, China;

[4]Yibin Meteorological Bureau, Yibin Sichuan 644000, China

Key Points:

- A significant multidecadal variability of autumn surface air temperature occurs over Southwest China (SWC).
- The Atlantic multidecadal oscillation (AMO) has a remote influence on the multidecadal variability of the autumn surface air temperature over Southwest China.
- The atmospheric Africa–Asia multidecadal teleconnection (AAMT) pattern associated with the AMO modulates the autumn surface air temperature over Southwest China.

Citation: Xu, W. L., Li, Y., Chen, Q. L., Zhou, X., Jiang, X. W., Wang, W., Huyan, L. D., Li, X., Jiang, Y. J., ... Zhu, Y. (2025). Remote influence of the Atlantic multidecadal oscillation on the autumn surface air temperature in Southwest China. *Earth Planet. Phys.*, *9*(5), 1061–1072. http://doi.org/10.26464/epp2025081

Abstract: Southwest China (SWC) is one of the major grain-producing areas in China, and the surface air temperature (SAT) during autumn has a substantial influence on grain production and planting. It is therefore important to understand temporal changes in the SAT over SWC (SWC-SAT). Our analysis of observational and reanalysis datasets shows that the autumn SWC-SAT exhibits significant multidecadal variability. A significantly strong positive correlation also exists between the autumn SWC-SAT and the Atlantic multidecadal oscillation (AMO) time series (correlation coefficient of 0.85). These results suggest that the AMO is a remote driver of multidecadal variability in the autumn SWC-SAT. Further analyses show that the North Atlantic sea surface temperature anomalies (SSTA) associated with the AMO modulate the multidecadal variability of the autumn SWC-SAT through triggering the Africa–Asia multidecadal teleconnection (AAMT) pattern. Specifically, the AAMT corresponds to geopotential height anomalies over SWC, which adjust the local thickness of the air column and thereby induce multidecadal variability of the autumn SWC-SAT. This potential mechanism, derived from observational and reanalysis datasets, was verified by using a linear barotropic model and the Community Atmosphere Model version 4. Our results from combining observations and numerical modeling simulations indicate that the North Atlantic SSTA may act as a key pacemaker for the multidecadal SAT variability over SWC.

Keywords: Southwest China; Atlantic multidecadal oscillation; surface air temperature; multidecadal variability

1. Introduction

The Atlantic multidecadal oscillation (AMO) is a key contributor to multidecadal climate variability on Earth. This variability is characterized by the spatially consistent pattern of the North Atlantic basin-wide warm or cold sea surface temperature anomaly (SSTA), which has a period of 50–70 years (Kerr, 2000; Enfield et al., 2001; Li S and Bates, 2007; Sutton and Hodson, 2007; Ting M et al., 2014; Sun C et al., 2017b; Zhang R et al., 2019). The AMO underwent warm phases in 1860–1880 and 1930–1960, whereas it shifted to cold phases in 1905–1925 and 1970–1990. Since the 1990s, it has gradually transitioned toward a warm phase (e.g., Gray et al., 2004; Li S and Bates, 2007; Zhang GW et al., 2020; Wang LC et al., 2023).

The persistent basin-scale SSTA associated with the AMO have important impacts on climate change over the North Atlantic and surrounding regions (e.g., Sutton and Hodson, 2005; Mariotti and Dell'Aquila, 2012; Muller et al., 2013; Drinkwater et al., 2014). The North Atlantic sea surface temperature (SST) has a warmer

First author: W. L. Xu, xuweiling_auto@163.com
Correspondence to: Y. Li, liyang0711@cuit.edu.cn
Q. L. Chen, chenql@cuit.edu.cn
Received 15 APR 2025; Accepted 26 MAY 2025.
First Published online 20 JUL 2025.

climatic mean state during summer and autumn (Frankignoul et al., 2003; Cattiaux et al., 2011; Sutton and Dong BW, 2012; Guo YP et al., 2016), and this may provide a warmer SST background and stronger coupling between the SST and convection (Seager and Murtugudde, 1997; Cheng KY et al., 2022; Huang P et al., 2024). The AMO has a substantial effect on the surface air temperature (SAT) and precipitation across Europe and North America, as well as on hurricane activity in the North Atlantic during summer and autumn (Enfield et al., 2001; Held and Soden, 2006; Knight et al., 2006). The North Atlantic SSTA associated with the AMO are likely to induce the generation of more hurricanes in the Atlantic Ocean, which in turn would affect the Atlantic climate (Enfield and CidSerrano, 2009). Nigam et al. (2011) used observations to show that the AMO has a substantial influence on the reconstruction of multiyear droughts and wet episodes over North America, particularly in the autumn wetness of the 1980s.

The AMO plays a key role in the global multidecadal variability of atmospheric circulation, temperature, and precipitation via atmospheric teleconnection (e.g., Dong BW et al., 2006; Zampieri et al., 2013; Li JP et al., 2019; Ratna et al., 2019; Zheng F et al., 2023). In addition to the North Atlantic and surrounding regions, the AMO also has a remote link to climate change in other regions over multidecadal timescales (Ratna et al., 2019; Xie TJ et al., 2019; Zhang R et al., 2019; Li JP et al., 2022). For example, the positive AMO phase can enhance the southeast and east Asian summer monsoons via a coupled air–sea interaction in the Indo-West Pacific region (Zhang R and Delworth, 2005; Lu RY et al., 2006). In addition, the AMO and its associated atmospheric Rossby wave propagation are the primary source of the multiyear prediction ability regarding the summer SAT over Northeast Asia (Monerie et al., 2018; Yeager et al., 2018).

Southwest China (SWC; 21°–35°N, 97°–112°E, Figure 1) comprises the provinces of Sichuan, Yunnan, Guizhou, and Guangxi, as well as the municipality of Chongqing (Qin NX et al., 2015; Zhu Y et al., 2024). Southwest China is one of the most densely populated regions in China, accounting for approximately 17% of the country's total population. It is also one of China's main grain-producing regions, accounting for approximately 16% of the national supply (Wang L et al., 2015). Using the annual mean temperature anomalies from 1880 to 2002, Wang SW et al. (2004) showed a multidecadal variation in the SWC temperature. Furthermore, Qian W and Qin A (2006) used national station observations from 1960 to 2000 to identify the multidecadal variability in the autumn SAT in SWC (SWC-SAT). The autumn SWC-SAT has followed a significant warming trend since the late 1990s (Liu XD and Chen BD, 2000; Ma ZF et al., 2013), which is consistent with the recent warm phase of the AMO. In paleoclimate studies using the reconstructed temperatures in SWC over the past millennium, results have suggested that the multidecadal variability of SWC temperatures is closely linked to the AMO (Wang JL et al., 2013, 2015; Shi SY et al., 2017; Fang KY et al., 2019).

In addition, several studies have found a statistical relationship between the AMO and multidecadal variability of the SWC-SAT over the past 50 years (e.g., Jin HY et al., 2022; Liu P et al., 2022; Deng KQ et al., 2024). However, we lack a systematic understanding

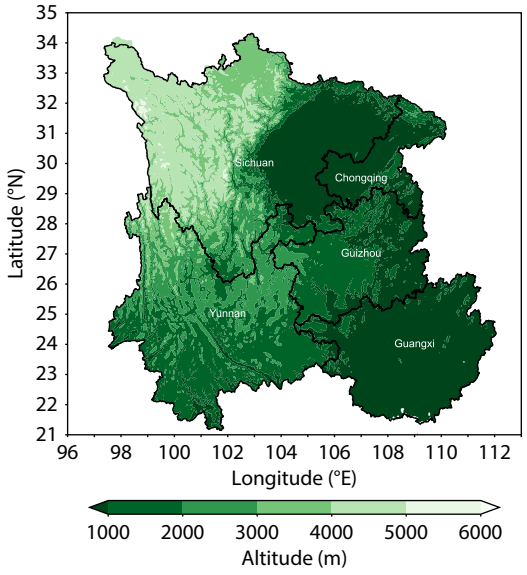

Figure 1. Topography and regions of SWC.

of how the AMO influences the SWC-SAT because the observational records are relatively short. In this study, we used a longer period of observations (i.e., the Climatic Research Unit [CRU] Time-Series [TS] version 4.08 and HadCRUT5 datasets) to calculate the correlation coefficient between the AMO and the SWC-SAT time series for each of the four seasons. The autumn correlation is the strongest (>0.85; statistically significant at the 95% confidence level). In SWC, autumn is the season when crops reach maturity and are harvested, while preparations are underway for planting winter crops.

During autumn, the SAT has a major impact on crop yields and the subsequent food supply (e.g., Bannayan et al., 2011; Rasul et al., 2011). Therefore, this article focuses on the multidecadal variability of the SWC-SAT and its linkage with the AMO. The remainder of this article is organized as follows. The data, methods, and models are described in Section 2, and the findings are presented in Section 3, focused on addressing the following questions:

(1) Does the autumn SWC-SAT show multidecadal variability?
(2) Does the AMO have a remote influence on multidecadal variability in the autumn SWC-SAT?
(3) If so, what is the mechanism that underlies this influence?
Finally, a summary and discussion are presented in Section 4.

2. Data and Methods

2.1 Data

We used the CRU TS version 4.08 temperature dataset with a horizontal resolution of 0.5° × 0.5° for the period of 1901–2023, obtained from the Climatic Research Unit at the University of East Anglia (Harris et al., 2020). The CRU TS dataset was created by interpolating monthly climate anomaly data from a global meteorological observation grid, using an angular-distance weighting method. The dataset is recognized as a reliable source of climate data for use in the analysis of global and East Asian climate change patterns and impacts (Buermann et al., 2018; Bromley et al., 2020; Li CX et al., 2020; Tan XZ et al., 2020). We calculated the

AMO and its associated SSTA by using the global sea surface ground temperature dataset HadCRUT5 from 1850 to the present. The HadCRUT5 dataset is collated by the Hadley Center of the UK Meteorological Office and the Climatic Research Unit at the University of East Anglia, and it has a horizontal resolution of 5° × 5° (Morice et al., 2021). The HadCRUT5 dataset is widely used to characterize the Atlantic SST in climate research (e.g., Qasmi, 2023; Schurer et al., 2023). For wind and geopotential height data, we used the 20th Century Reanalysis (version 2) dataset (20CRv2C) from the National Oceanic and Atmospheric Administration (NOAA) covering the period of 1851–2012 and with a horizontal resolution of 2° × 2°.

2.2 Methods

We defined the SWC-SAT time series as the area-weighted average of the SAT anomalies over SWC (21°–35°N, 97°–112°E). Following previous studies (Trenberth and Shea, 2006; Sun C et al., 2017a, b), we defined the AMO time series as the area-weighted mean of SSTA over the North Atlantic (0°–60°N, 0°–80°W). The Africa–Asia multidecadal teleconnection (AAMT) was identified in previous studies to explore the multidecadal teleconnection associated with the AMO (e.g., Sun C et al., 2017a; Li JP et al., 2019; Xie TJ et al., 2019). The AAMT index is the leading principal component (PC1) time series of empirical orthogonal function 1 (EOF1; approximately 30% variance), which is statistically significant (North et al., 1982). The EOF1 is calculated through the autumn meridional wind anomalies across the Eurasian continent (0°–60°N, 60°W–150°E) at 300 hPa (V300). Following previous studies (Sun C et al., 2017a), the V300 anomalies were smoothed by using an 11-year running mean filter to isolate the multidecadal signal before applying the EOF.

According to the hypsometric equation, the average temperature of the atmosphere between pressures p_1 and p_2 can be expressed as follows (Wallace et al., 1996; Holton and Gregory, 2013):

$$\langle T\rangle = \frac{g_0}{R}\left(\ln\frac{p_1}{p_2}\right)^{-1}\Delta Z, \tag{1}$$

$$\Delta Z = Z_2 - Z_1,$$

where $\langle T\rangle$ is the average temperature of the atmospheric layer, ΔZ is the thickness of the atmosphere, and Z_1 and Z_2 are the geopotential height at the p_1 and p_2, respectively. The gravitational acceleration is g_0 = 9.80655 m·s^{-2} and the dry air gas constant is R = 287 J·kg^{-1}·K^{-1} in the equation above. If we consider $\langle T\rangle'$ and $\Delta Z'$ as deviations or anomalies from their mean value, Equation (1) can be rewritten as a perturbation equation, as follows:

$$\langle T\rangle' = \frac{g_0}{R}\left(\ln\frac{p_1}{p_2}\right)^{-1}\Delta Z'. \tag{2}$$

Equation (2) shows that the anomalous mean temperature between the pressure levels is proportional to the anomalous thickness of the layer. This equation can be used to investigate the impact of upper-level atmospheric circulation on changes in the SAT (Wallace et al., 1996; Zhang YZ et al., 2022).

The statistical significance of the correlation between two autocorrelated time series is calculated using the two-tailed Student's t-test and the effective number of degrees of freedom ($N^{\rm eff}$) (Pyper and Peterman, 1998; Li JP et al., 2013), as follows:

$$\frac{1}{N^{\rm eff}} \approx \frac{1}{N} + \frac{2}{N}\sum_{j=1}^{N}\frac{N-j}{N}\rho_{XX}(j)\rho_{YY}(j), \tag{3}$$

where N is the number of samples, and $\rho_{XX}(j)$ and $\rho_{YY}(j)$ denote the autocorrelations of the time series X and Y, at time lag j, respectively.

Prior to the analysis, all variables and indices were linearly detrended using the least squares method, which removes centennial-scale trends to better isolate and highlight the signal associated with the multidecadal variability. Because this study focuses on multidecadal timescales, we smoothed the data by using an 11-year Gaussian low-pass filter for most of our analysis. We also used power spectral analysis, lead–lag correlation, and linear regression methods. The autumn variables were calculated as the mean values for September, October, and November, and the anomalies represent the deseasonalized anomalies with respect to the period of 1961–1990.

2.3 Model Experiment

To investigate the mechanism underlying the atmospheric teleconnection pattern, we used the linear barotropic model (LBM) to analyze the atmospheric response to the thermal forcing related to the AMO. The LBM is a linearized atmospheric model developed to improve our understanding of the complex feedback mechanisms within the atmosphere by eliminating nonlinear atmospheric processes (Watanabe, 2005). Further details regarding the model formulation can be found in Watanabe and Kimoto (2000). The LBM simulates the stable linear response of the atmosphere to specific forcings (Held et al., 2002), and the model has a T42 horizontal spectral resolution and 20 vertical levels. Note that the LBM is typically used to explore the atmospheric teleconnection pattern over Eurasia (Lu RY and Lin ZD, 2009; Yasui and Watanabe, 2010; Sun C et al., 2014). The spatial distribution and vertical structure of the thermal forcing associated with the AMO over the North Atlantic is shown in Figure S1.

We also used the Community Atmosphere Model version 4 (CAM4), which is the atmospheric component of the Global Circulation Model (GCM) and Community Earth System Model (CESM), developed by the National Center for Atmospheric Research (NCAR; Neale et al., 2013). The CAM4 is the atmospheric component of the CESM. The CAM4 has a medium-resolution version (1.9° × 2.5°) that includes 96 longitude and 144 latitude points. The CAM4 has been widely used to study the response of the atmospheric circulation to SST (He ZQ and Wu RG, 2014; Koenigk et al., 2019). This model can better reproduce the temperature distribution and its seasonal variation characteristics in China (e.g., Yu ET et al., 2018). We undertook two groups of experiments: a control run (i.e., EXP0) forced by the 30-year average SST of the global climate state, and a sensitivity run (i.e., EXP1) that included an AMO-related SST forcing in the North Atlantic. Note that both the control and sensitivity experiments were based on case F_2000, in which the solar forcing, carbon dioxide, ozone concentration, and aerosol are fixed at the year 2000 level. The details of the experiments are provided in Table 1.

Table 1. Detailed design of the CAM4 experiments.

Experiment	Description
EXP0	Control run using case F_2000. Prescribed SST forcing based on the climatological present-day SST provided by NCAR.
EXP1	AMO sensitivity run. Same as EXP0, but with SST anomalies associated with the AMO (Figure S2) added over the North Atlantic (0°–60°N, 0°–80°W) during autumn.

3. Results

3.1 Multidecadal Variability in the Autumn SWC-SAT and Its Linkage to the AMO

To reveal the multidecadal variability in the autumn SWC-SAT, we analyzed the SWC-SAT anomalies averaged over the region 21°–35°N, 97°–112°E for the period of 1901–2023. Figure 2a shows the raw and 11-year Gaussian low-pass filtered time series for the autumn SWC-SAT. Both time series show well-defined multidecadal variations, with cold phases around 1901–1915 and 1950–1990, and warm phases around 1915–1950 and after 1990 (Figure 2a). To further elucidate the predominant periodicities associated with the autumn SWC-SAT, the power spectrum of the autumn SWC-SAT time series is shown in Figure 2b. The SWC-SAT exhibits a significant (at the 95% confidence level) spectral peak with a period of approximately 60 years (Figure 2b), which is consistent with the AMO period (e.g., Enfield et al., 2001; Sutton and Hodson, 2007). These results motivated us to study the potential linkage between the autumn SWC-SAT and the AMO.

We followed the approach of previous studies that have defined the AMO (e.g., Trenberth and Shea, 2006; Sun C et al., 2017a) to calculate the autumn AMO time series. To detect the potential linkage between the AMO and the autumn SWC-SAT, we plotted the detrended and 11-year Gaussian low-pass filtered time series of the autumn AMO and SWC-SAT together (Figure 2c). Both the filtered SWC-SAT time series and the AMO (Figure 2c) show pronounced multidecadal variability, and the multidecadal fluctuations of the SWC-SAT appear to be approximately in phase with those of the AMO. Specifically, the filtered time series of the

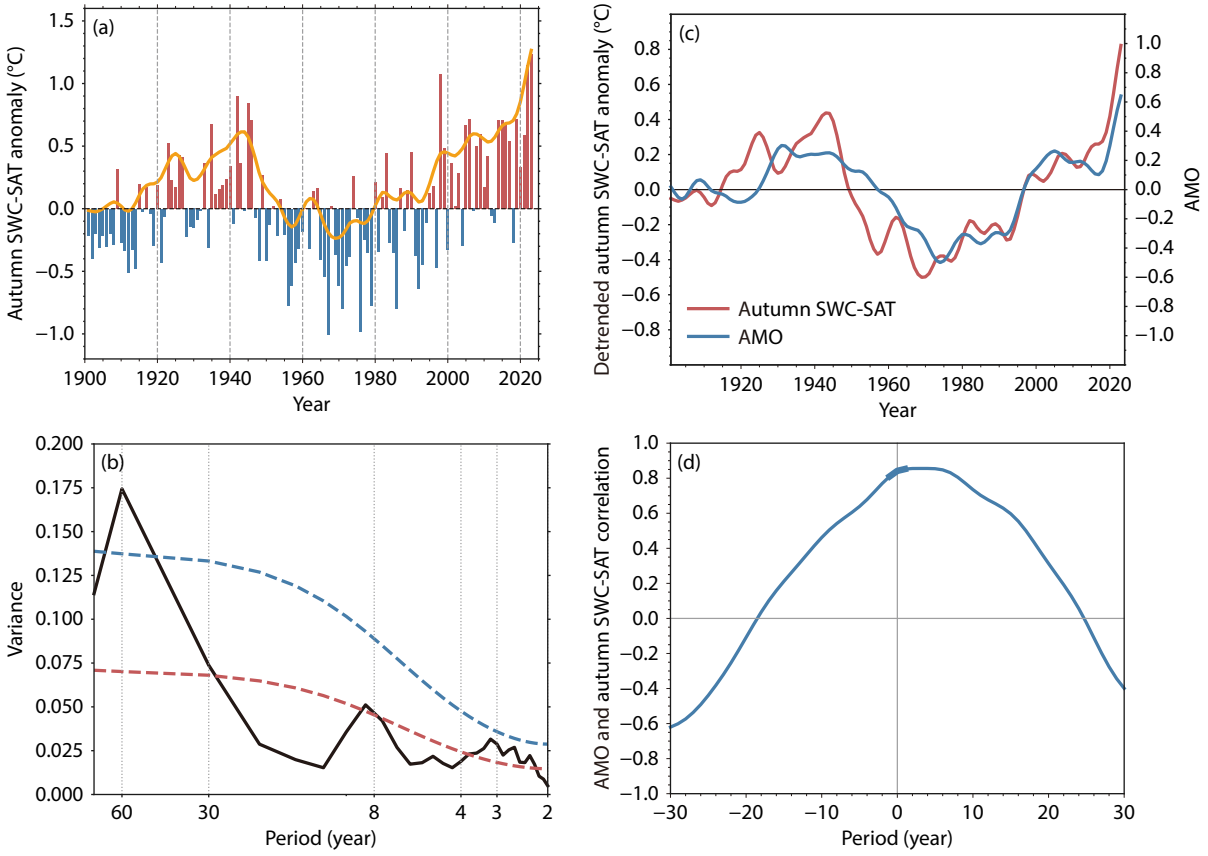

Figure 2. (a) Area-averaged autumn SWC-SAT anomalies (bars) and the 11-year Gaussian low-pass filtered (orange line) time series over the period of 1901–2023 based on the CRU TS version 4.08 dataset. (b) Power spectrum of the autumn SWC-SAT anomalies for the period of 1900–2023. The blue and red dashed lines show the 95% confidence level and the reference red noise spectrum, respectively. (c) Detrended time series of the autumn SWC-SAT anomalies (red line) and the AMO (blue line) from 1901 to 2023 after applying an 11-year Gaussian low-pass filter. (d) Lead–lag correlation between the detrended autumn AMO and the SWC-SAT time series over the period of 1901–2023 after applying an 11-year Gaussian low-pass filter. Negative (positive) lags indicate that the autumn AMO leads (lags) the SWC-SAT, and the thick blue line indicates statistical significance at the 95% confidence level when using the effective number of degrees of freedom.

autumn SWC-SAC and AMO are in their negative phase between 1950 and 2000 and in positive phases before 1950 and after 2000. Figure 2d further shows the lead–lag correlation between the filtered SWC-SAT time series and the AMO index. A strong correlation is evident between the filtered SWC-SAT and the AMO time series at zero lag (correlation coefficient of ~0.85, significant at the 95% confidence level). This result indicates that the multidecadal variability in the SWC-SAT may be largely explained by the AMO.

We further investigated the spatial pattern of the relationship between the AMO and the SWC-SAT. Figure 3a shows the correlation map between the AMO time series and the SWC-SAT anomalies during autumn. The SAT anomalies and the AMO are significantly correlated over the entire SWC region, with correlation coefficients mostly above 0.7 and being significant at the 95% confidence level. These results suggest that the multidecadal variability of the SWC-SAT is closely related to the AMO.

In addition to the AMO, the interdecadal Pacific oscillation (IPO; Power et al., 1999; Folland et al., 2002; IPCC, 2013a; Henley et al., 2015) and the Pacific decadal oscillation (PDO; Mantua et al., 1997; IPCC, 2013b) are important climatic modes at decadal to multidecadal timescales, although there remains debate regarding the difference between the IPO and PDO (e.g., Holbrook et al., 2014). Previous studies have reported that the IPO and PDO influence global and regional SATs (e.g., Dong B and Dai AG, 2015; Meehl et al., 2016; Henley et al., 2017). On the basis of these points, we considered whether the IPO or PDO signal could influence the relationship between the AMO and the autumn SWC-SAT. To clarify the possible impact of the IPO (PDO), we first removed the IPO (PDO) signal and then performed a correlation analysis between the AMO time series and the SWC-SAT. Specifically, to remove the IPO (PDO) signal, the autumn SWC-SAT anomalies were regressed onto the AMO time series and the result was then subtracted from the total SWC-SAT anomalies. Note that it is challenging to completely remove the variations related to a specific variable from the climate records because of the nonlinear influences; thus, our results might exclude only the linear components (e.g., Li Y et al., 2019).

Figures 3b and 3c show the spatial pattern of the correlation coefficients between the AMO and the autumn SWC-SAT without the IPO signal (Figure 3b) or PDO signal (Figure 3c). It can clearly be seen that the correlation maps without the IPO and PDO (Figures 3b and 3c) are similar to the raw correlation map (Figure 3a). That is, significant correlation coefficients remain between the AMO and the autumn SWC-SAT even after removing the IPO or PDO signals over the entire SWC region (Figures 3b and 3c). In addition, the correlation coefficients without the IPO or PDO signal (Figures 3b and 3c) are weaker than the raw correlation (Figure 3a) in SWC. This result implies that the IPO and PDO contribute to the multidecadal variability of the autumn SWC-SAT. However, the IPO and PDO may explain only part of the multidecadal variability in the autumn SWC-SAT because the correlation coefficients calculated without the IPO or PDO signals exceed 0.5 across the entire SWC region. These results suggest that neither the IPO signal nor the PDO signal is able to affect the robust link between the AMO and the autumn SWC-SAT and that the AMO has a remote influence on the multidecadal variability of the autumn SWC-SAT.

3.2 Potential Mechanism for the Remote Influence of the AMO on Multidecadal Variability in the Autumn SWC-SAT

Here, we investigated the remote influence of the AMO on the multidecadal variability of the autumn SWC-SAT. Previous studies have reported that the AMO plays a vital role in multidecadal climate change in the northern hemisphere by triggering the AAMT, which acts as an atmospheric bridge, conveying the influence of the AMO onto the downstream multidecadal variation (e.g., Li JP et al., 2013, 2022; Sun C et al., 2017a). To investigate the spatial pattern of the AAMT, we calculated the meridional wind at 300 hPa (V300) regressed onto the AAMT time series on a multidecadal timescale (Figure 4a). Note that the correlation coefficient between the autumn AMO and AAMT time series is high (>0.71, statistically significant at the 99% confidence level), indicating a strong in-phase relationship between them (e.g., Sun C et al., 2017a). As shown in Figure 4a, the AAMT wave train has three positive centers and three negative centers from Africa to East Asia between 20°N and 40°N, which is similar to the findings of previous studies (e.g., Sun C et al., 2017a; Xie TJ et al., 2019). In

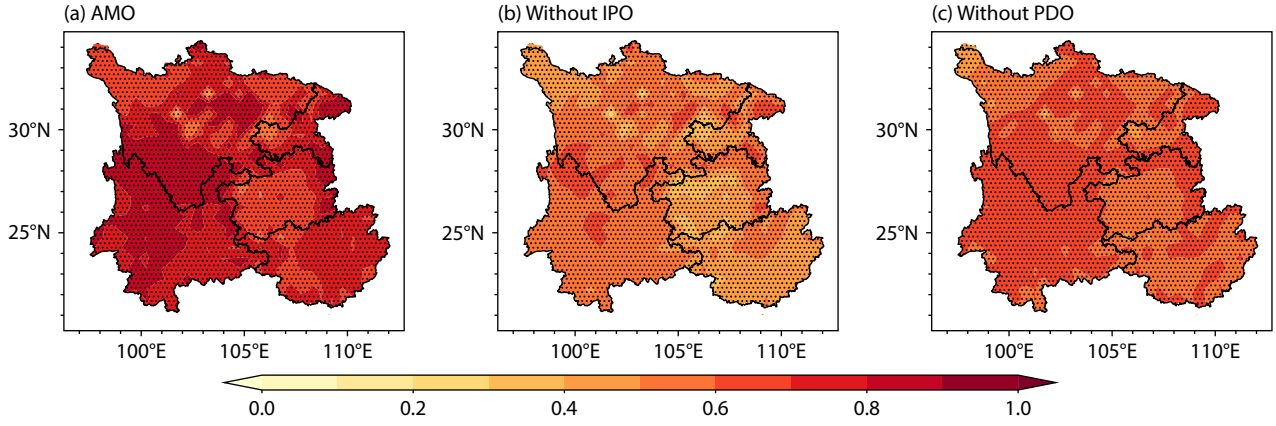

Figure 3. (a) Correlation map between the autumn 11-year Gaussian low-pass filtered AMO time series and the SWC-SAT over the period of 1901–2023. (b, c) As for (a), but after removal of the IPO signal or the PDO signal, respectively. The dotted areas indicate correlations significant at the 95% confidence level.

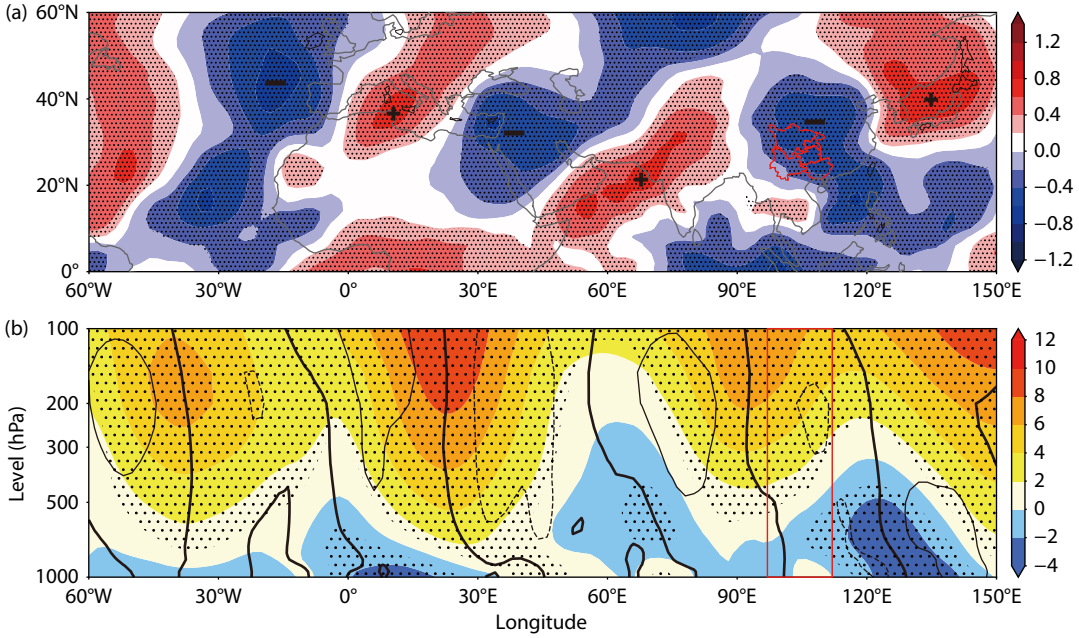

Figure 4. V300 and geopotential height anomalies regressed onto the AAMT index. (a) Spatial pattern of the 11-year Gaussian low-pass filtered autumn meridional wind at 300 hPa (V300) anomalies over the Eurasian continent (0°–60°N, 60°W–150°E) from 1900 to 2012 regressed onto the normalized time series of the autumn AAMT. (b) Autumn meridional wind (contours, meters per second) and geopotential height anomalies (shading, meters) across 20°–35°N regressed onto the normalized time series of the autumn AAMT from 1900 to 2012. The zero contour of meridional wind anomalies (0) is shown as a solid bold line, the positive contours (+0.3) as solid lines, and the negative contours (−0.3) as dashed lines. The red rectangle indicates the longitudinal range of the SWC region. The dotted areas indicate that the regressions for height are statistically significant at the 95% confidence level when using the effective number of degrees of freedom.

particular, the only negative center of the AAMT wave train over East Asia is located in the SWC region. Given that the AMO can excite the AAMT wave train (e.g., Sun C et al., 2017a; Li JP et al., 2022), it is suggested that the AMO may have impacts on the SWC-SAT through the AAMT.

To investigate the potential mechanism associated with the remote influence of the AMO on the multidecadal variability of the autumn SWC-SAT, we first analyzed the vertical structure of the autumn AAMT. Figure 4b shows the latitudinal averages of geopotential height and meridional wind anomalies regressed onto the AAMT time series during the period of 1901–2012. Note that the latitudinal averages in Figure 4b were calculated within the band 20°–35°N, which covers the entire SWC region. As shown in Figure 4b, the meridional wind pattern related to the AAMT has relatively large values of meridional wind in the upper troposphere. The vertical structure of the geopotential height is broadly consistent with that of the meridional wind, showing three positive regions in the upper troposphere extending from the northwest coast of Africa to the SWC region.

According to Equation (2) and previous studies (e.g., Wallace et al., 1996; Sun C et al., 2016; Li Y et al., 2024; Zhu Y et al., 2024), the tropospheric upper-level geopotential height anomalies can modulate the tropospheric temperature through the air thickness and thus influence the SAT. Figure 5a shows a correlation map between the autumn AAMT time series and air thickness from 1000 hPa to the upper level (1000–300 hPa). The thickness pattern is positively correlated with the AAMT over the entire SWC region (Figure 5a). The strong correlation between the AMO and AAMT time series (correlation coefficient of >0.71) indicates that the positive AMO phase corresponds to the increasing thickness over the entire SWC region, which is caused by the greater geopotential height at the upper level than at the lower level (Figure 4b). Because the tropospheric temperature is related to the thickness based on the hypsometric equation (Equation (2)), the warming temperature related to the AAMT is expected to be modified by the increasing thickness. The spatial correlation map of tropospheric temperature shows positive values over the entire SWC region (Figure 5b), highlighting the warming temperature associated with the AAMT or positive AMO phase. In addition, the correlation map of tropospheric temperature (Figure 5b) is in good agreement with that of the SAT over the SWC region (Figure 5c). This agreement arises mainly from the strong coupling of air temperature from the troposphere to the surface (e.g., Wallace et al., 1996; Sun C et al., 2016).

These results imply that the AAMT associated with the AMO influence the multidecadal variability of the autumn SWC-SAT. To further clarify the remote influence of the AMO on the autumn SWC-SAT via the AAMT, we recalculated the correlation map between the AMO and autumn SWC-SAT, but for the SAT without the AAMT signal (using the regression method as in Figures 3b and 3c). When the correlation maps with the AAMT signal (Figure 3a) and without the AAMT signal (Figure 5d) were compared, the correlation values without the AAMT signal were much weaker and the correlation coefficients were 0.2 over the entire SWC region (Figure 5d). This result further suggests that the AAMT

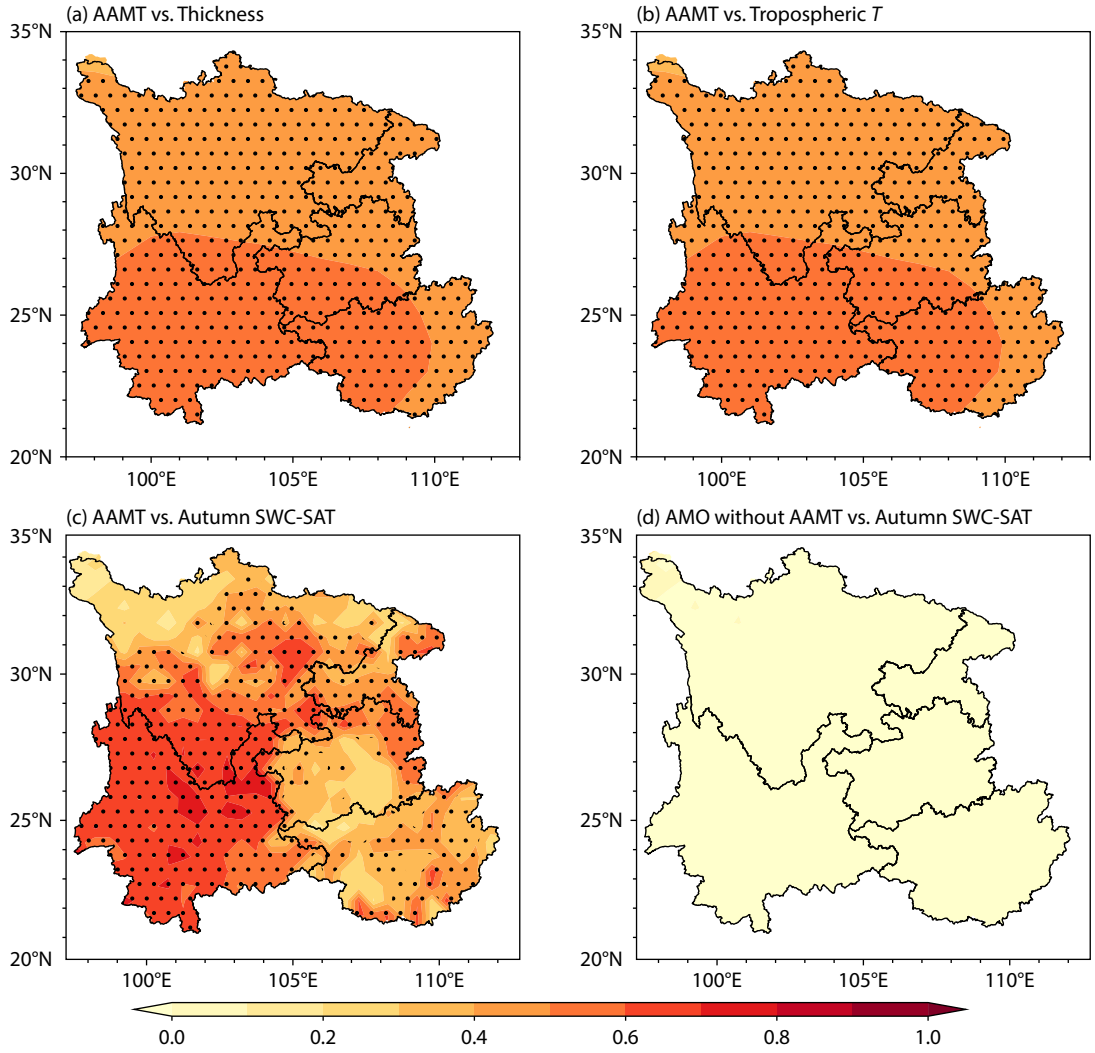

Figure 5. (a) Correlation map between the autumn 11-year Gaussian low-pass filtered AAMT time series and air thickness from 1000 to 300 hPa for the period of 1901–2012. (b) Correlation map between the autumn 11-year Gaussian low-pass filtered AAMT time series and the tropospheric temperature calculated using the air thickness between 1000 and 300 hPa. (c) Correlation map between the autumn 11-year Gaussian low-pass filtered AAMT time series and autumn SWC-SAT for the period of 1901–2012. (d) As for (c), but for the AAMT time series after removal of the AMO signals. The dotted areas indicate correlations that are statistically significant at the 90% confidence level.

plays a vital role in the remote influence of the AMO on the multi-decadal variability of the autumn SWC-SAT.

3.3 Modeling Evidence for the Remote Influence of the AMO

The results above suggest that a remote teleconnection exists between the AMO and the SWC-SAT. To further verify the associated mechanism, we performed an LBM experiment. In this study, the model was forced with a prescribed thermal forcing pattern representing the heating over the North Atlantic associated with the AMO (Figure S1). Figure 6a shows the LBM-simulated response of the atmosphere to the heat forcing associated with the AMO and that the LBM-simulated AAMT pattern (Figure 6a) is roughly consistent with the observed AAMT (Figure 4a). The LBM experiment was able to capture the only negative V300 center within the East Asian region, although there is a northward shift in the location of this negative center when compared with the observations (Figure 6a). This simulated bias is probably the result of the LBM being a simplified linear model.

In addition to the LBM experiment, we performed control and sensitivity CAM4 experiments (Table 1) to further support our results. Figure 6b shows the V300 response to the SST anomalies associated with the positive phase of the AMO during autumn in the CAM4 simulations. The positive AMO corresponds to the atmospheric teleconnection (Figure 6b), which is in good agreement with both the observed (Figure 4a) and LBM-simulated (Figure 6a) AAMT. Note that CAM4 also reproduced the only negative center over the East Asian region, which covers the SWC region (Figure 6b). Compared with the LBM simulation, this negative center over SWC simulated by CAM4 is closer in position to that in the observations (Figures 6a and 6b), which may be related to the relatively complex atmospheric process of CAM4 (e.g., Neale et al., 2013). Regarding the vertical structure of the AAMT, CAM4 was also able to capture the main features and show the larger geopotential height in the upper troposphere (Figure 6c).

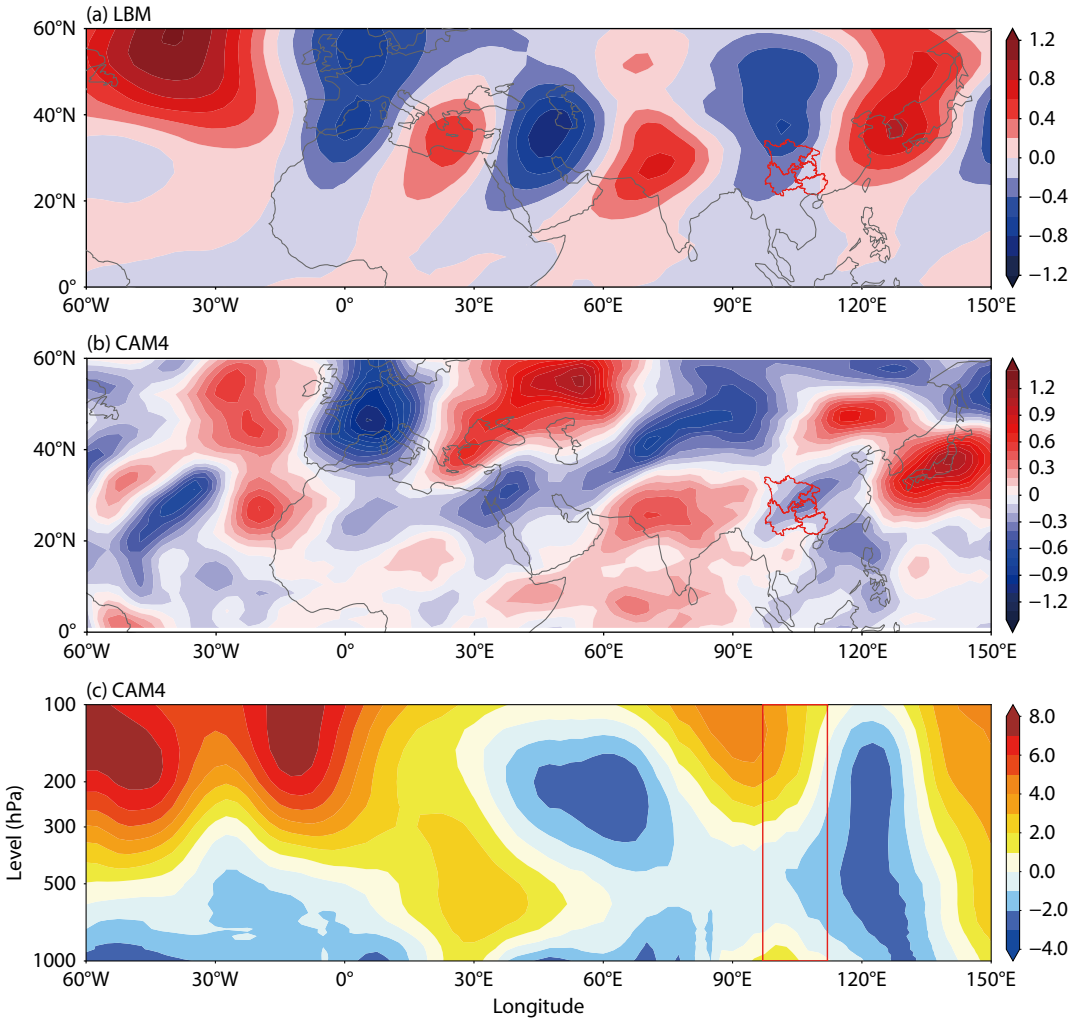

Figure 6. (a) LBM simulation of the steady responses of the autumn meridional wind at V300 anomalies (contours, meters per second) to the Atlantic thermal forcing. (b) CAM4 simulation of the autumn meridional wind at V300 anomalies over the Eurasian continent (0°–60°N, 60°W–150°E). (c) CAM4 simulation of the autumn geopotential height anomalies (shading, meters) at 20°–35°N. The red rectangle indicates the longitudinal range of the SWC region.

According to the hypsometric equation (Equation (2)), this simulated teleconnection would also induce the warming of the SWC-SAT (Figure S3). When the observations (Figure 4) were compared with the model simulations (Figure 6), some biases were found within the LBM and CAM4 simulations, likely related to the incomplete representation of complex atmospheric processes in the models. Nevertheless, the model simulations give us confidence that the LBM and CAM4 reproduced the observed anomalous atmospheric teleconnection associated with the AMO to a large extent and that the simulated high geopotential height in the upper troposphere contributes to the warming SWC-SAT.

4. Conclusions and Discussion

In this study, we used the CRU TS version 4.08 and HadCRUT5 datasets to investigate the remote influence of the AMO on the multidecadal variability of the autumn SAT over SWC and the associated mechanism. We found that the autumn SWC-SAT shows well-defined multidecadal variations, with a significant 60-year cycle, which is consistent with the AMO period. To understand the link between the autumn SWC-SAT and the AMO, we calculated their lead–lag correlation. The lead–lag correlation between the filtered autumn SWC-SAT time series and the AMO index was high (correlation coefficient of 0.85) at zero lag and was statistically significant at the 95% confidence level (two-tailed Student's *t*-test; Figure 2d). These results imply that the AMO has a robust remote influence on the multidecadal variability of the autumn SWC-SAT, which is unaffected by the IPO and PDO signals (Figures 3a and 3c).

To study the potential mechanisms associated with the remote influence of the AMO on the multidecadal variability of the autumn SWC-SAT, we regressed the meridional wind at 300 hPa (V300) onto the AAMT time series over a multidecadal period (Figure 4a). The AAMT wave train has three positive centers and three negative centers from Africa to East Asia between 20°N and 40°N. Of note, the SWC region is located on the only negative center of V300 associated with the AAMT wave train in East Asia. In addition, the vertical structure related to the AAMT shows three positive geopotential height anomalies in the upper troposphere, extending from the northwest coast of Africa to the SWC region.

According to the atmospheric thickness formulae (Equation (2)) and previous studies (Wallace et al., 1996; Sun C et al., 2017b; Li Y et al., 2024; Zhu Y et al., 2024), the tropospheric upper-level geopotential height anomalies could modulate the tropospheric temperature via the air thickness and thereby influence the SAT. Considering the strong correlation between the AMO and the AAMT time series (>0.71), our results suggest that the AAMT associated with the AMO corresponds to the upper-level positive center of geopotential height over SWC, which modulates the tropospheric temperature through the air thickness and subsequently affects the SAT. To further verify our observational results, we designed and performed the LBM (Figure 6a) and CAM4 (Figures 6b and 6c) experiments to evaluate the influence of the AMO. Both the LBM and CAM4 models were able to simulate an AAMT pattern that was essentially consistent with the observed AAMT (Figure 4a). The two models also captured the negative V300 center over the East Asian region. The vertical structure of the AAMT was also reproduced, with relatively larger geopotential heights simulated in the upper troposphere over SWC (Figure 6c).

This study focused primarily on the remote influence of the AMO on the multidecadal variability of the autumn SWC-SAT when using both observations and model simulations. The IPO and PDO may also contribute to this multidecadal variability in autumn SWC-SAT (Figures 3b and 3c), although they have no effect on the stable connection between the autumn SWC-SAT and the AMO. Future work is needed to improve our understanding of the relative contributions of the AMO, IPO, and PDO to changes in the SWC-SAT.

CRediT Authorship Contribution Statement

WeiLing Xu: Writing—original draft, Visualization, Formal analysis. Yang Li: Conceptualization, Formal analysis, Writing—review & editing, Funding acquisition, Supervision. QuanLiang Chen: Writing—review & editing, Funding acquisition. Xin Zhou: Writing—review & editing, Funding acquisition. XingWen Jiang: Writing—review & editing. Wei Wang: Writing—review & editing. LiDou Huyan: Writing—review & editing. Xiao Li: Writing—review & editing. YangJie Jiang: Data curation. RuiHan Deng: Data curation. GuiPing Zhang: Writing—review & editing. Yun Zhu: Formal analysis.

Declaration of Competing Interests

The authors declare that they have no conflicts of interest.

Acknowledgments

This work was jointly supported by the National Natural Science Foundation of China (Grant Nos. U2442210, 42175042, and 42275059), the Natural Science Foundation of Sichuan Province (Grant No. 2024NSFTD0017), the Second Tibetan Plateau Scientific Expedition and Research (STEP) program (Grant No. 2019QZKK0103), and the Natural Science Foundation of Chongqing (Grant No. cstc2021jcyj-msxmX0698).

Data and Materials Availability

The monthly CRU TS dataset can be downloaded from https://crudata.uea.ac.uk/cru/data/hrg/cru_ts_4.08/. The monthly HadCRUT5 dataset can be downloaded from https://www.metoffice.gov.uk/hadobs/hadcrut5/. The 20th Century Reanalysis version 2 dataset can be downloaded from NOAA-CIRES 20th Century Reanalysis (V2c): NOAA Physical Sciences Laboratory NOAA-CIRES 20th Century Reanalysis (V2c).

References

Bannayan, M., Lotfabadi, S. S., Sanjani, S., Mohamadian, A., and Aghaalikhani, M. (2011). Effects of precipitation and temperature on crop production variability in northeast Iran. *Int. J. Biometeorol.*, *55*(3), 387–401. https://doi.org/10.1007/s00484-010-0348-7

Bromley, G. T., Gerken, T., Prein, A. F., and Stoy, P. C. (2020). Recent trends in the near-surface climatology of the northern North American Great Plains. *J. Climate*, *33*(2), 461–475. https://doi.org/10.1175/jcli-d-19-0106.1

Buermann, W., Forkel, M., O'Sullivan, M., Sitch, S., Friedlingstein, P., Haverd, V., Jain, A. K., Kato, E., Kautz, M., … Richardson, A. D. (2018). Widespread seasonal compensation effects of spring warming on northern plant productivity. *Nature*, *562*(7725), 110–114. https://doi.org/10.1038/s41586-018-0555-7

Cattiaux, J., Vautard, R., and Yiou, P. (2011). North-Atlantic SST amplified recent wintertime European land temperature extremes and trends. *Climate Dyn.*, *36*(11), 2113–2128. https://doi.org/10.1007/s00382-010-0869-0

Cheng, K. Y., Harris, L., Bretherton, C., Merlis, T. M., Bolot, M., Zhou, L. J., Kaltenbaugh, A., Clark, S., and Fueglistaler, S. (2022). Impact of warmer sea surface temperature on the global pattern of intense convection: Insights from a global storm resolving model. *Geophys. Res. Lett.*, *49*(16), e2022GL099796. https://doi.org/10.1029/2022GL099796

Deng, K. Q., Yang, S., Fan, K., Wang, Z. Q., Yu, W., Huang, Z. Y., Xia, M., Chen, D. L., Lian, T., and Tian, B. Q. (2024). A dry–wet teleconnection between southwestern and northeastern China in winter and early spring. *Climate Dyn.*, *62*(7), 6643–6663. https://doi.org/10.1007/s00382-024-07228-9

Dong, B., and Dai, A. G. (2015). The influence of the Interdecadal Pacific Oscillation on temperature and precipitation over the globe. *Climate Dyn.*, *45*(9-10), 2667–2681. https://doi.org/10.1007/s00382-015-2500-x

Dong, B. W., Sutton, R. T., and Scaife, A. A. (2006). Multidecadal modulation of El Niño–Southern Oscillation (ENSO) variance by Atlantic Ocean sea surface temperatures. *Geophys. Res. Lett.*, *33*(8), L08705. https://doi.org/10.1029/2006gl025766

Drinkwater, K. F., Miles, M., Medhaug, I., Otterå, O. H., Kristiansen, T., Sundby, S., and Gao, Y. Q. (2014). The Atlantic Multidecadal Oscillation: Its manifestations and impacts with special emphasis on the Atlantic region north of 60°N. *J. Mar. Syst.*, *133*, 117–130. https://doi.org/10.1016/j.jmarsys.2013.11.001

Enfield, D. B., Mestas-Nuñez, A. M., and Trimble, P. J. (2001). The Atlantic Multidecadal Oscillation and its relation to rainfall and river flows in the continental U. *S. Geophys. Res. Lett.*, *28*(10), 2077–2080. https://doi.org/10.1029/2000gl012745

Enfield, D. B., and CidSerrano, L. (2009). Secular and multidecadal warmings in the North Atlantic and their relationships with major hurricane activity. *Int. J. Climatol.*, *30*(2), 174–184. https://doi.org/10.1002/joc.1881

Fang, K. Y., Guo, Z. T., Chen, D. L., Wang, L., Dong, Z. P., Zhou, F. F., Zhao, Y., Li, J. B., Li, Y. J., and Cao, X. G. (2019). Interdecadal modulation of the Atlantic Multi-decadal Oscillation (AMO) on southwest China's temperature over the past 250 years. *Climate Dyn.*, *52*(3-4), 2055–2065. https://doi.org/10.1007/s00382-018-4244-x

Folland, C. K., Renwick, J. A., Salinger, M. J., and Mullan, A. B. (2002). Relative influences of the Interdecadal Pacific Oscillation and ENSO on the South Pacific Convergence Zone. *Geophys. Res. Lett.*, *29*(13), 1643. https://doi.org/10.1029/2001gl014201

Frankignoul, C., Friederichs, P., and Kestenare, E. (2003). Influence of Atlantic SST anomalies on the atmospheric circulation in the Atlantic-European sector. *Annals. Geophys.*, *46*(1), 71–85. https://doi.org/10.4401/ag-3390

Gray, S. T., Graumlich, L. J., Betancourt, J. L., and Pederson, G. T. (2004). A tree-

ring based reconstruction of the Atlantic Multidecadal Oscillation since 1567 A. D. *Geophys. Res. Lett.*, *31*(12), L12205. https://doi.org/10.1029/2004gl019932

Guo, Y. P., Li, J. P., Feng, J., Xie, F., Sun, C., and Zheng, J. Y. (2016). The multidecadal variability of the asymmetric mode of the boreal autumn Hadley circulation and its link to the Atlantic multidecadal oscillation. *J. Climate*, *29*(15), 5625–5641. https://doi.org/10.1175/jcli-d-15-0025.1

Harris, I., Osborn, T. J., Jones, P., and Lister, D. (2020). Version 4 of the CRU TS monthly high-resolution gridded multivariate climate dataset. *Sci. Data*, *7*(1), 109. https://doi.org/10.1038/s41597-020-0453-3

He, Z. Q., and Wu, R. G. (2014). Indo-Pacific remote forcing in summer rainfall variability over the South China Sea. *Climate Dyn.*, *42*(9-10), 2323–2337. https://doi.org/10.1007/s00382-014-2123-7

Held, I. M., Ting, M., and Wang, H. L. (2002). Northern winter stationary waves: Theory and modeling. *J. Climate*, *15*(16), 2125–2144. https://doi.org/10.1175/1520-0442(2002)015<2125:NWSWTA>2.0.CO;2

Held, I. M., and Soden, B. J. (2006). Robust responses of the hydrological cycle to global warming. *J. Climate*, *19*(21), 5686–5699. https://doi.org/10.1175/jcli3990.1

Henley, B. J., Gergis, J., Karoly, D. J., Power, S., Kennedy, J., and Folland, C. K. (2015). A tripole index for the Interdecadal Pacific Oscillation. *Climate Dyn.*, *45*(11-12), 3077–3090. https://doi.org/10.1007/s00382-015-2525-1

Henley, B. J., Meehl, G., Power, S. B., Folland, C. K., King, A. D., Brown, J. N., Karoly, D. J., Delage, F., Gallant, A. J. E., … Neukom, R. (2017). Spatial and temporal agreement in climate model simulations of the Interdecadal Pacific Oscillation. *Environ. Res. Lett.*, *12*(4), 044011. https://doi.org/10.1088/1748-9326/aa5cc8

Holbrook, N. J., Li, J. P., Collins, M., Di Lorenzo, E., Jin, F. F., Knutson, T., Latif, M., Li, C., Power, S. B., and Huang, R. (2014). Decadal climate variability and cross-scale interactions: ICCL 2013 expert assessment workshop. *Bull. Amer. Meteor. Soc.*, *95*(8), ES155–ES158. https://doi.org/10.1175/BAMS-D-13-00201.1

Holton, J. R., and Gregory J. H. (2013). An Introduction to Dynamic Meteorology (Vol. 88). Amsterdam: Academic Press.

Huang, P., Chen, Y., Li, J. B., and Yan, H. (2024). Redefined background state in the tropical Pacific resolves the entanglement between the background state and ENSO. *npj. Climate Atmos. Sci.*, *7*(1), 147. https://doi.org/10.1038/s41612-024-00695-1

IPCC. (2013a). Near-term climate change: Projections and predictability. In IPCC (Ed.), *Climate Change 2013–The Physical Science Basis. Contribution of Working Group I to the Fifth Assessment Report of the Intergovernmental Panel on Climate Change* (pp. 953–1028). Cambridge, UK: Cambridge University Press.

IPCC. (2013b). Climate Phenomena and their Relevance for Future Regional Climate Change. In: *Climate Change 2013: The Physical Science Basis. Contribution of Working Group I to the Fifth Assessment Report of the Intergovernmental Panel on Climate Change* (pp. 1217–1308). Cambridge, UK: Cambridge University Press.

Jin, H. Y., Cheng, Q. P., and Wang, P. (2022). Three-dimensional dynamic variations of ground/air surface temperatures and their correlation with large-scale circulation indexes in southwest China (1980–2019). *Atmosphere*, *13*(7), 1031. https://doi.org/10.3390/atmos13071031

Kerr, R. A. (2000). A North Atlantic climate pacemaker for the centuries. *Science*, *288*(5473), 1984–1985. https://doi.org/10.1126/science.288.5473.1984

Knight, J. R., Folland, C. K., and Scaife, A. A. (2006). Climate impacts of the Atlantic Multidecadal Oscillation. *Geophys. Res. Lett.*, *33*(17), L17706. https://doi.org/10.1029/2006gl026242

Koenigk, T., Gao, Y., Gastineau, G., Keenlyside, N., Nakamura, T., Ogawa, F., Orsolini, Y., Semenov, V., Suo, L. … Yang, S. (2019). Impact of Arctic sea ice variations on winter temperature anomalies in northern hemispheric land areas. *Climate Dyn.*, *52*(5-6), 3111–3137. https://doi.org/10.1007/s00382-018-4305-1

Li, C. X., Wang, C. Z., and Zhao, T. B. (2020). Seasonal covariability of dryness or wetness in China and global sea surface temperature. *J. Climate*, *33*(2), 727–747. https://doi.org/10.1175/jcli-d-19-0250.1

Li, J. P., Sun, C., and Jin, F. F. (2013). NAO implicated as a predictor of Northern Hemisphere mean temperature multidecadal variability. *Geophys. Res. Lett.*, *40*(20), 5497–5502. https://doi.org/10.1002/2013gl057877

Li, J. P., Zheng, F., Sun, C., Feng, J., and Wang, J. (2019). Pathways of influence of the northern hemisphere mid–high latitudes on East Asian climate: A review. *Adv. Atmos. Sci.*, *36*(9), 902–921. https://doi.org/10.1007/s00376-019-8236-5

Li, J. P., Xie, T. J., Tang, X. X., Wang, H., Sun, C., Feng, J., Zheng, F., and Ding, R. Q. (2022). Influence of the NAO on wintertime surface air temperature over East Asia: Multidecadal variability and decadal prediction. *Adv. Atmos. Sci.*, *39*(4), 625–642. https://doi.org/10.1007/s00376-021-1075-1

Li, S. L., and Bates, G. T. (2007). Influence of the Atlantic Multidecadal Oscillation on the winter climate of East China. *Adv. Atmos. Sci.*, *24*, 126–135. https://doi.org/10.1007/s00376-007-0126-6

Li, Y., Chen, Q. L., Liu, X. R., Li, J. P., Xing, N., Xie, F., Feng, J., Zhou, X., Cai, H. K., and Wang, Z. L. (2019). Long-term trend of the tropical Pacific trade winds under global warming and its causes. *J. Geophys. Res.: Oceans*, *124*(4), 2626–2640. https://doi.org/10.1029/2018JC014603

Li, Y., Feng, W. H., Zhou, X., Li, Y. J., and Chipperfield, M. P. (2024). The impact of El Niño–Southern Oscillation on the total column ozone over the Tibetan Plateau. *Atmos. Chem. Phys.*, *24*(14), 8277–8293. https://doi.org/10.5194/acp-24-8277-2024

Liu, P., Zhang, Y., and Tang, M. Y. (2022). Effects of Atlantic multidecadal oscillation and Pacific decadal oscillation on interdecadal variability of fog frequency in autumn–winter season in Southwest China. *Int. J. Climatol.*, *42*(4), 2083–2098. https://doi.org/10.1002/joc.7353

Liu, X. D., and Chen, B. D. (2000). Climatic warming in the Tibetan Plateau during recent decades. *Int. J. Climatol.*, *20*(14), 1729–1742. https://doi.org/10.1002/1097-0088(20001130)20:14<1729::Aid-joc556>3.0.Co;2-y

Lu, R. Y., Dong, B. W., and Ding, H. (2006). Impact of the Atlantic Multidecadal Oscillation on the Asian summer monsoon. *Geophys. Res. Lett.*, *33*(24), L24701. https://doi.org/10.1029/2006GL027655

Lu, R. Y., and Lin, Z. D. (2009). Role of subtropical precipitation anomalies in maintaining the summertime meridional teleconnection over the western North Pacific and East Asia. *J. Climate*, *22*(8), 2058–2072. https://doi.org/10.1175/2008JCLI2444.1

Ma, Z. F., Liu, J., Zhang, S. Q., Chen, W. X., and Yang, S. Q. (2013). Observed climate changes in Southwest China during 1961–2010. *Adv. Climate Change Res.*, *4*(1), 30–40. https://doi.org/10.3724/sp.J.1248.2013.030

Mantua, N. J., Hare, S. R., Zhang, Y., Wallace, J. M., and Francis, R. C. (1997). A Pacific interdecadal climate oscillation with impacts on salmon production. *Bull. Amer. Meteor. Soc.*, *78*(6), 1069–1079. https://doi.org/10.1175/1520-0477(1997)078<1069:Apicow>2.0.Co;2

Mariotti, A., and Dell'Aquila, A. (2012). Decadal climate variability in the Mediterranean region: Roles of large-scale forcings and regional processes. *Climate Dyn.*, *38*(5-6), 1129–1145. https://doi.org/10.1007/s00382-011-1056-7

Meehl, G. A., Hu, A. X., and Teng, H. Y. (2016). Initialized decadal prediction for transition to positive phase of the Interdecadal Pacific Oscillation. *Nat. Commun.*, *7*(1), 11718. https://doi.org/10.1038/ncomms11718

Monerie, P. A., Robson, J., Dong, B. W., and Dunstone, N. (2018). A role of the Atlantic Ocean in predicting summer surface air temperature over North East Asia?. *Climate Dyn.*, *51*, 473–491. https://doi.org/10.1007/s00382-017-3935-z

Morice, C. P., Kennedy, J. J., Rayner, N. A., Winn, J. P., Hogan, E., Killick, R. E., Dunn, R. J. H., Osborn, T. J., Jones, P. D., and Simpson, I. R. (2021). An updated assessment of near-surface temperature change from 1850: The HadCRUT5 data set. *J. Geophys. Res.: Atmos.*, *126*(3), e2019JD032361. https://doi.org/10.1029/2019jd032361

Muller, R. A., Curry, J., Groom, D., Jacobsen, R., Perlmutter, S., Rohde, R., Rosenfeld, A., Wickham, C., and Wurtele, J. (2013). Decadal variations in the

global atmospheric land temperatures. *J. Geophys. Res.: Atmos.*, *118*(11), 5280–5286. https://doi.org/10.1002/jgrd.50458

Neale, R. B., Richter, J., Park, S., Lauritzen, P. H., Vavrus, S. J., Rasch, P. J., and Zhang, M. H. (2013). The mean climate of the Community Atmosphere Model (CAM4) in forced SST and fully coupled experiments. *J. Climate*, *26*(14), 5150–5168. https://doi.org/10.1175/JCLI-D-12-00236.1

Nigam, S., Guan, B., and Ruiz-Barradas, A. (2011). Key role of the Atlantic Multidecadal Oscillation in 20th century drought and wet periods over the Great Plains. *Geophys. Res. Lett.*, *38*(16), L16713. https://doi.org/10.1029/2011gl048650

North, G. R., Bell, T. L., Cahalan, R. F., and Moeng, F. J. (1982). Sampling errors in the estimation of empirical orthogonal functions. *Mon. Wea. Rev.*, *110*(7), 699–706. https://doi.org/10.1175/1520-0493(1982)110<0699:SEITEO>2.0.CO;2

Power, S., Casey, T., Folland, C., Colman, A., and Mehta, V. (1999). Inter-decadal modulation of the impact of ENSO on Australia. *Climate Dyn.*, *15*(5), 319–324. https://doi.org/10.1007/s003820050284

Pyper, B. J., and Peterman, R. M. (1998). Comparison of methods to account for autocorrelation in correlation analyses of fish data. *Can. J. Fish. Aquat. Sci.*, *55*(9), 2127–2140. https://doi.org/10.1139/f98-104

Qasmi, S. (2023). Past and future response of the North Atlantic warming hole to anthropogenic forcing. *Earth Syst. Dyn.*, *14*(3), 685–695. https://doi.org/10.5194/esd-14-685-2023

Qian, W., and Qin, A. (2006). Spatial-temporal characteristics of temperature variation in China. *Meteor. Atmos. Phys.*, *93*(1-2), 1–16. https://doi.org/10.1007/s00703-005-0163-6

Qin, N. X., Wang, J. N., Yang, G. S., Chen, X., Liang, H. Y., and Zhang, J. B. (2015). Spatial and temporal variations of extreme precipitation and temperature events for the Southwest China in 1960–2009. *Geoenviron. Dis.*, *2*(1), 4. https://doi.org/10.1186/s40677-015-0014-9

Rasul, G., Chaudhry, Q. Z., Mahmood, A., and Hyder, K. W. (2011). Effect of temperature rise on crop growth & productivity. *Pak. J. Meteor.*, *8*(15), 53–62.

Ratna, S. B., Osborn, T. J., Joshi, M., Yang, B., and Wang, J. L. (2019). Identifying teleconnections and multidecadal variability of East Asian surface temperature during the last millennium in CMIP5 simulations. *Climate Past*, *15*(5), 1825–1844. https://doi.org/10.5194/cp-15-1825-2019

Schurer, A. P., Hegerl, G. C., Goosse, H., Bollasina, M. A., England, M. H., Smith, D. M., and Tett, S. F. B. (2023). Role of multi-decadal variability of the winter North Atlantic Oscillation on Northern Hemisphere climate. *Environ. Res. Lett.*, *18*(4), 044046. https://doi.org/10.1088/1748-9326/acc477

Seager, R., and Murtugudde, R. (1997). Ocean dynamics, thermocline adjustment, and regulation of tropical SST. *J. Climate*, *10*(3), 521–534. https://doi.org/10.1175/1520-0442(1997)010<0521:ODTAAR>2.0.CO;2

Shi, S. Y., Li, J. B., Shi, J. F., Zhao, Y. S., and Huang, G. (2017). Three centuries of winter temperature change on the southeastern Tibetan Plateau and its relationship with the Atlantic Multidecadal Oscillation. *Climate Dyn.*, *49*(4), 1305–1319. https://doi.org/10.1007/s00382-016-3381-3

Sun, C., Li, J. P., Jin, F. F., and Xie, F. (2014). Contrasting meridional structures of stratospheric and tropospheric planetary wave variability in the Northern Hemisphere. *Tellus A: Dyn. Meteor. Oceanogr.*, *66*(1), 25303. https://doi.org/10.3402/tellusa.v66.25303

Sun, C., Li, J. P., and Ding, R. Q. (2016). Strengthening relationship between ENSO and western Russian summer surface temperature. *Geophys. Res. Lett.*, *43*(2), 843–851. https://doi.org/10.1002/2015gl067503

Sun, C., Li, J. P., Ding, R. Q., and Jin, Z. (2017a). Cold season Africa–Asia multidecadal teleconnection pattern and its relation to the Atlantic multidecadal variability. *Climate Dyn.*, *48*(11-12), 3903–3918. https://doi.org/10.1007/s00382-016-3309-y

Sun, C., Kucharski, F., Li, J. P., Jin, F. F., Kang, I. S., and Ding, R. Q. (2017b). Western tropical Pacific multidecadal variability forced by the Atlantic multidecadal oscillation. *Nat. Commun.*, *8*(1), 15998. https://doi.org/10.1038/ncomms15998

Sutton, R. T., and Hodson, D. L. R. (2005). Atlantic Ocean forcing of North American and European summer climate. *Science*, *309*(5731), 115–118. https://doi.org/10.1126/science.1109496

Sutton, R. T., and Hodson, D. L. R. (2007). Climate response to basin-scale warming and cooling of the North Atlantic Ocean. *J. Climate*, *20*(5), 891–907. https://doi.org/10.1175/jcli4038.1

Sutton, R. T., and Dong, B. W. (2012). Atlantic Ocean influence on a shift in European climate in the 1990s. *Nat. Geosci.*, *5*(11), 788–792. https://doi.org/10.1038/ngeo1595

Tan, X. Z., Wu, Y., Liu, B. J., and Chen, S. L. (2020). Inconsistent changes in global precipitation seasonality in seven precipitation datasets. *Climate Dyn.*, *54*(5-6), 3091–3108. https://doi.org/10.1007/s00382-020-05158-w

Ting, M., Kushnir, Y., and Li, C. H. (2014). North Atlantic Multidecadal SST Oscillation: External forcing versus internal variability. *J. Mar. Syst.*, *133*, 27–38. https://doi.org/10.1016/j.jmarsys.2013.07.006

Trenberth, K. E., and Shea, D. J. (2006). Atlantic hurricanes and natural variability in 2005. *Geophys. Res. Lett.*, *33*(12), L12704. https://doi.org/10.1029/2006GL026894

Wallace, J. M., Zhang, Y., and Bajuk, L. (1996). Interpretation of interdecadal trends in Northern Hemisphere surface air temperature. *J. Climate*, *9*(2), 249–259. https://doi.org/10.1175/1520-0442(1996)009<0249:IOITIN>2.0.CO;2

Wang, J. L., Yang, B., Qin, C., Kang, S. Y., He, M. H., and Wang, Z. Y. (2013). Tree-ring inferred annual mean temperature variations on the southeastern Tibetan Plateau during the last millennium and their relationships with the Atlantic Multidecadal Oscillation. *Climate Dyn.*, *43*(3-4), 627–640. https://doi.org/10.1007/s00382-013-1802-0

Wang, J. L., Yang, B., and Ljungqvist, F. C. (2015). A millennial summer temperature reconstruction for the eastern Tibetan Plateau from tree-ring width. *J. Climate*, *28*(13), 5289–5304. https://doi.org/10.1175/jcli-d-14-00738.1

Wang, L., Chen, W., Zhou, W., and Huang, G. (2015). Drought in southwest China: A review. *Atoms. Ocean Sci. Lett.*, *8*(6), 339–344. https://doi.org/10.3878/AOSL20150043

Wang, L. C., Gu, X. H., Slater, L. J., Li, J. F., Kong, D. D., Zhang, X., and Liu, J. Y. (2023). Phase shifts of the PDO and AMO alter the translation distance of global tropical cyclones. *Earth's Future*, *11*(3), e2022EF003079. https://doi.org/10.1029/2022EF003079

Wang, S. W., Zhu, J. H., and Cai, J. N. (2004). Interdecadal variability of temperature and precipitation in China since 1880. *Adv. Atmos. Sci.*, *21*(3), 307–313. https://doi.org/10.1007/BF02915560

Watanabe, M., and Kimoto, M. (2000). Atmosphere-ocean thermal coupling in the North Atlantic: A positive feedback. *Quart. J. Roy. Meteor. Soc.*, *126*(570), 3343–3369. https://doi.org/10.1002/qj.49712657017

Watanabe, M. (2005). *Linear Baroclinic Model (LBM) Package*. https://www.aoml.noaa.gov/ftp/pub/phod/sklee/public/hyunsoo/LBM_manual.

Xie, T. J., Li, J. P., Sun, C., Ding, R. Q., Wang, K. C., Zhao, C. F., and Feng, J. (2019). NAO implicated as a predictor of the surface air temperature multidecadal variability over East Asia. *Climate Dyn.*, *53*(1-2), 895–905. https://doi.org/10.1007/s00382-019-04624-4

Yasui, S., and Watanabe, M. (2010). Forcing processes of the summertime circumglobal teleconnection pattern in a dry AGCM. *J. Climate*, *23*(8), 2093–2114. https://doi.org/10.1175/2009JCLI3323.1

Yeager, S. G., Danabasoglu, G., Rosenbloom, N. A., Strand, W., Bates, S. C., Meehl, G. A., Karspeck, A. R., Lindsay, K., Long, M. C., … Lovenduski, N. S. (2018). Predicting near-term changes in the Earth system: A large ensemble of initialized decadal prediction simulations using the community Earth system model. *Bull. Amer. Meteor. Soc.*, *99*(9), 1867–1886. https://doi.org/10.1175/BAMS-D-17-0098.1

Yu, E. T., Zhang, R., Jiang, D. B., Ramstein, G., Zhang, Z. S., and Sun, J. Q. (2018). High-resolution simulation of Asian monsoon response to regional uplift of the Tibetan Plateau with regional climate model nested with global climate

model. *Global Planet. Change*, *169*, 34–47. https://doi.org/10.1016/j.gloplacha.2018.07.002

Zampieri, M., Scoccimarro, E., and Gualdi, S. (2013). Atlantic influence on spring snowfall over the Alps in the past 150 years. *Environ. Res. Lett.*, *8*(3), 034026. https://doi.org/10.1088/1748-9326/8/3/034026

Zhang, G. W., Zeng, G., Li, C., and Yang, X. Y. (2020). Impact of PDO and AMO on interdecadal variability in extreme high temperatures in North China over the most recent 40-year period. *Climate Dyn.*, *54*(5), 3003–3020. https://doi.org/10.1007/s00382-020-05155-z

Zhang, R., and Delworth, T. L. (2005). Simulated tropical response to a substantial weakening of the Atlantic thermohaline circulation. *J. Climate*, *18*(12), 1853–1860. https://doi.org/10.1175/JCLI3460.1

Zhang, R., Sutton, R., Danabasoglu, G., Kwon, Y. O., Marsh, R., Yeager, S. G., Amrhein, D. E., and Little, C. M. (2019). A review of the role of the Atlantic meridional overturning circulation in Atlantic multidecadal variability and associated climate impacts. *Rev. Geophys.*, *57*(2), 316–375. https://doi.org/10.1029/2019RG000644

Zhang, Y. Z., Li, J. P., Hou, Z. L., Zuo, B., Xu, Y. D., Tang, X. X., and Wang, H. (2022). Climatic effects of the Indian Ocean tripole on the western United States in boreal summer. *J. Climate*, *35*(8), 2503–2523. https://doi.org/10.1175/jcli-d-21-0490.1

Zheng, F., Liu, X. N., Chen, J. H., Huang, W., Sun, C., and Wang, H. (2023). Physical mechanism of winter temperature multidecadal variations in arid Central Asia: The role of the Atlantic Multidecadal Oscillation (AMO). *J. Climate*, *36*(21), 7363–7377. https://doi.org/10.1175/JCLI-D-22-0946.1

Zhu, Y., Li, Y., Zhou, X., Feng, W. H., Gao, G. L., Li, M. G., and Zheng, G. W. (2024). Causes of the severe drought in southwest China during the summer of 2022. *Atmos. Res.*, *303*, 107320. https://doi.org/10.1016/j.atmosres.2024.107320